REPORT DOCUMENTATION PAGE

1. REPORT DATE (DD-MM-YYYY) 03-05-2011	2. REPORT TYPE	3. DATES COVERED (From - To)

4. TITLE AND SUBTITLE

Analysis of Transient and Steady State Neutral Flows in a Field Reversed

Configuration Thruster

5a. CONTRACT NUMBER

5b. GRANT NUMBER

5c. PROGRAM ELEMENT NUMBER

6. AUTHOR(S)

Ryan Jansen, Jean-Luc Cambier, Sergey Gimelshein, and David Kirtley

5d. PROJECT NUMBER

5f. WORK UNIT NUMBER
2308M132

7. PERFORMING ORGANIZATION NAME(S) AND ADDRESS(ES)

Air Force Research Laboratory (AFMC)
AFRL/RZSA
10 E. Saturn Blvd.
Edwards AFB CA 93524-7680

8. PERFORMING ORGANIZATION REPORT NUMBER

AFRL-RZ-ED-TP-2011-199

9. SPONSORING / MONITORING AGENCY NAME(S) AND ADDRESS(ES)

Air Force Research Laboratory (AFMC)
AFRL/RZS
5 Pollux Drive
Edwards AFB CA 93524-7048

10. SPONSOR/MONITOR'S ACRONYM(S)

11. SPONSOR/MONITOR'S NUMBER(S)
AFRL-RZ-ED-TP-2011-199

12. DISTRIBUTION / AVAILABILITY STATEMENT

Approved for public release; distribution unlimited (PA #11227).

13. SUPPLEMENTARY NOTES
For presentation at the AIAA Plasmadynamics and Lasers conference, Honolulu, HI, 01 Jul 2011.

14. ABSTRACT

A combined Navier-Stokes/DSMC approach is used to compute a neutral injection into a field reversed configuration thruster. Transient flow is studied for different thruster geometries, gases, and chamber conditions. Flow uniformity inside the diverging conical nozzle is analyzed for both transient and steady state thruster operations.

15. SUBJECT TERMS

16. SECURITY CLASSIFICATION OF:			17. LIMITATION OF ABSTRACT	18. NUMBER OF PAGES	19a. NAME OF RESPONSIBLE PERSON Dr. Ingrid J. Wysong
a. REPORT Unclassified	b. ABSTRACT Unclassified	c. THIS PAGE Unclassified	SAR	12	19b. TELEPHONE NUMBER (include area code) N/A

Analysis of Transient and Steady State Neutral Flows in a Field Reversed Configuration Thruster

Ryan Jansen[*]

University of Southern California, Los Angeles, CA 91205

Jean-Luc Cambier [†]

Air Force Research Laboratory, Edwards AFB, CA 93524

Sergey Gimelshein[‡]

ERC, Inc., Edwards AFB, CA 93524

David Kirtley[§]

MSNW, Redmond, WA 98052

A combined Navier-Stokes/DSMC approach is used to compute a neutral injection into a field reversed configuration thruster. Transient flow is studied for different thruster geometries, gases, and chamber conditions. Flow uniformity inside the diverging conical nozzle is analyzed for both transient and steady state thruster operation.

High-power electric propulsion is an enabling technology for future space missions, but one that also presents a number of technical challenges. First, it is critically important to operate a thruster at very high efficiency, otherwise the system limitations due to heat rejection become insurmountable. Second, high power can be efficiently delivered into a plasma by raising its temperature (provided radiative losses are not excessive), i.e. its specific energy; consequently, the specific impulse can take large values, even in the excess of 10,000 sec. The optimal conditions from the standpoint of low radiation loss, acceptable ionization cost, and confinement requirements, are usually achieved for low-Z plasma at high (50-100 eV) temperature and in strong magnetic fields. These conditions are typically obtained in Field Reversed Configuration (FRC) (see, for example, Ref. 1) plasma. The FRC is a self-organized magnetized plasma structure in the shape of a highly compact toroid. The magnetic field is mostly in the poloidal direction,[2] generated by internal (toroidal) currents. The ratio of plasma pressure to magnetic pressure is close to unity, i.e. the highest plasma density that can be attained for given external magnets. The poloidal field also contributes to the particle confinement. Starting from a background uniform plasma at a constant axial (bias) field, the FRC can be formed by pulsing external coils and reversing the applied field, inducing currents at the plasma boundary and "pinching" the plasma at both ends (see Fig. 1). The initial bias field is trapped inside the plasma and forced to reconnect at the end points (separatrix), creating an elongated toroidal shape.

In contrast to some other high I_{sp} plasma propulsion concepts,[3] the FRC is completely magnetically insulated from the external field: the plasma is not tied to an external field line, and the FRC can readily detach from the confining external field. It can also be translated and accelerated by applying a gradient of magnetic pressure using pulsed external coils. The FRC can therefore be efficiently accelerated to provide thrust, operates at a temperature that is optimal for ionization and is well confined. The basic concept of operations has been demonstrated[4] and more recent research has led to further optimization of the formation process,[5] while methods for increased efficiency through energy recovery in the electrical circuits are currently

---

[*]Undergraduate Student, Astronautical Engineering
[†]Senior Scientist, Propulsion Directorate
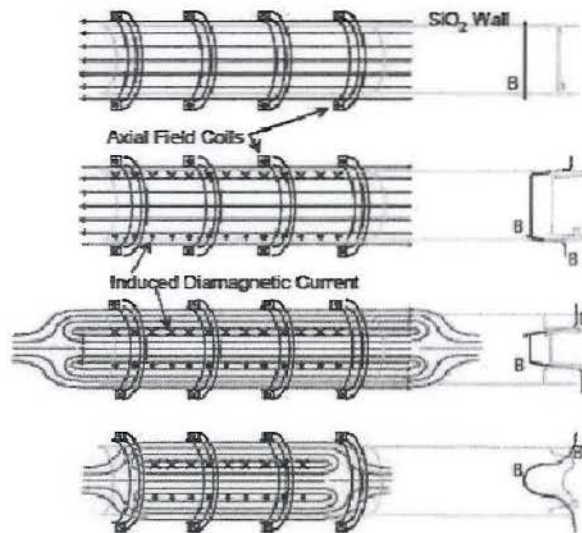[‡]Consultant
[§]Scientist

Figure 1. Schematic of basic FRC formation by field reversal.

being developed. One of the latest design iterations[6] provides plasma velocities in the 10-40 km/sec range, a desirable regime for USAF applications. However, many aspects of the flow development and device operation, such as power and mass utilization efficiencies, still remain to be determined more precisely.

An important aspect of device operation and efficiency is the initial distribution of carrier gas in the throat and in the pre-ionization and the main FRC chambers immediately before the pre-ionization. The main goal of this paper is to study the impact of different operational parameters, such as the FRC chamber geometry, stagnation pressure, carrier gas, and the puff valve opening time, on the uniformity of gas density in the main chamber, as well as the gas flow properties in the pre-ionization chamber. The work addresses the sensitivity of gas properties to the above parameters and studies both transient and steady-state gas flows.

I. Geometry and Flow Conditions

In this work, the geometrical setup of experimental studies[6,7] is used. The setup is shown in Fig. 2a (all dimensions are given in millimeters). The working gas from the stagnation chamber through a 1 mm diameter orifice into a 6.35 mm diameter and 88.9 mm long tube, then it flow around a cylindrical 6.35 mm diameter electrode into an annular 60 mm long pre-ionization chamber. In the experimental setup, gas was supplied to the pre-ionization chamber through four 90-degree azimuthal holes with 1.5 mm diameters. Preliminary numerical analysis have shown that it is extremely difficult, if not impossible, to obtain transient 3D solutions converged in terms of grid and time step. Since accuracy of simulations is important, an equivalent axially symmetric configuration has been used in the present work. The four azimuthal holes were replaced by an annular configuration. Two different flow areas were considered, the one that a constriction with an opening area equal to that in the experiments (a spacing of 0.5 mm), and the one that has a two times larger opening (a spacing of 0.25 mm), and thus a length-to-spacing ratio closer to the experimental value. After the pre-ionization chamber, the gas flows in the main diverging nozzle where the FRC plasmoid will be formed and then propelled out. The nozzle has a 20 deg diverging conical section and a total length of 318 mm and exit diameter of 258 mm.

Three stagnation pressures were considered, 7.5 psi, 15 psi, and 30 psi, with the constant stagnation temperature of 300 K. The carrier gas was molecular nitrogen in all cases except for one where neon was used. Transient evolution of gas flow was followed from the valve opening (time 0) to 5 ms. It is important that, similar to the experiments,[6,7] the valve was assumed open only for 420 μs, after which it was instantaneously

close. Since the valve closing in the experiment is not instantaneous, a calculation with valve open during the first 320 μs was also conducted. The steady state solution is also presented in order to provide the information on a possible quasi-steady state thruster operation.
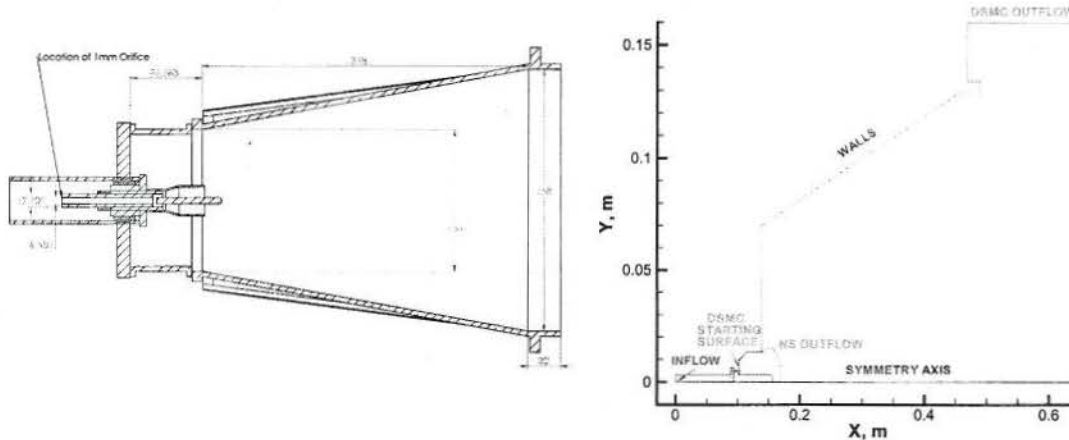

Figure 2. Drawing of the FRC thruster[6] (left) and the schematics of the numerical setup (right).

II.   Numerical Approach

The gas pressure is expected to vary greatly as the carrier gas leaves the stagnation chamber and passes through the inlet to the pre-ionization chamber and out to the main nozzle, typically decreasing from a few atmosphere level to a small fraction of a Pascal. This dictates a combined use of a continuum and kinetic approaches, with the continuum approach applied to the flow through the inlet, and a kinetic method used in the pre-ionization chamber and the diverging nozzle. In this work, the solution of the Navier-Stokes equations was used for the inlet flow, and the DSMC method for the flow in the pre-ionization chamber and diverging nozzle. A one-way coupling between these approaches is used, with the interface surface between the two approaches set in the vicinity of the inlet into the pre-ionization chamber. The location of the interface surface was chosen so that the flow is supersonic, and the gas density is low enough for the DSMC method to be feasible, and still high enough for the continuum approach to be applicable. The schematics of the numerical setup is given in Fig. 2b. The CFD++ solver is applied in the region that start with the gas inflow and stretches to the exit from the pre-ionization chamber to the diverging nozzle (marked as Navier-Stokes outflow). The DSMC computational domain begins from the starting surface and propagates to the plume near field (marked as DSMC outflow). Note that there is an overlap region where both approaches were used; it covers most of the pre-ionization chamber and allows for code-to code comparison. For transient flow simulations, which are the main topic of this work, the gas properties along the interface surface are stored at different time moments (typically every 10 μs), and a 5-th order Lagrange polynomial interpolation is then used in the kinetic simulation to determine the actual gas properties at every time moment at every point of the interface surface.

The computational tool used for the solution of the Navier-Stokes equations is CFD++[8] developed by Metacomp Technologies, Inc. CFD++ is a flexible computational fluid dynamics software suite for the solution of steady and unsteady, compressible and incompressible Navier-Stokes equations, including multi-species capability for perfect and reacting gases. In this work, a turbulent Reynolds Averaged Navier-Stokes capability of CFD++ is applied. The simulations were conducted with a 2nd order in space, Harten, Lax, van Leer, Contact discontinuity Riemann approximation algorithm. The computations that utilize a two-equation $k - \epsilon$ turbulence model will be presented. Implicit time integration was used. A real gas model (nitrogen) was used here. The surface was assumed isothermal with a constant temperature of 300 K. Second order slip boundary conditions were applied at the wall.

The axisymmetric capability of the DSMC-based code SMILE[9] has been used as the principal kinetic approach. The important features of SMILE that are relevant to this work are parallel capability, different collision and macroparameter grids with manual and automatic adaptations, and spatial weighting for axisymmetric flows. The majorant frequency scheme was used to calculate intermolecular interactions. The intermolecular potential was assumed to be a variable hard sphere. Energy redistribution in molecular collisions between the internal and translational modes was performed in accordance with the Larsen-Borgnakke model. Temperature-dependent relaxation numbers were used. The reflection of molecules on the surface was assumed to be diffuse with complete energy and momentum accommodation (except for one case shown below where a specular reflection was imposed).

III.   Convergence and numerical accuracy

The convergence study has been conducted in order to obtain results not biased by the cell size and time step (as well as the number of molecules in the DSMC simulations). For the Navier-Stokes solver, the sensitivity of macroparameters to the cell size both in the axial and radial direction, and the time step was analyzed, and the time step and cell size were decreased until there was no visible change in the flow properties. An example of the convergence results is shown in Fig. 3 where the gas pressure is shown obtained by CFD++ at two different time moments after the valve opening. Here and below in this section, the results are shown for 5 psig chamber pressure and a 0.5 mm annular constriction spacing case (see the *Geometry and flow conditions* section). In the standard resolution case (top), about 150,000 cells were used, with cell resolution varying throughout the domain and in the axial and radial direction, and a time step of 1 ns was chosen. In the high resolution case, the time step increased from 0.25 ns during the first 0.4 ms to 0.5 ns and then af6ter 1 ms after valve opening to 1 ns. The cell size was up to 50% lower both in axial and radial direction. It can be sse from the figure that the difference between the two solutions is very small at 0.42 ms (there is some minor difference inside the inlet tube and in the shock reflections in the pre-ionization chamber), and even smaller at 2 ms (at that time, it is noticeable only in the inlet tube). The convergence was considered satisfactory, and standard resolution used in all subsequent runs.
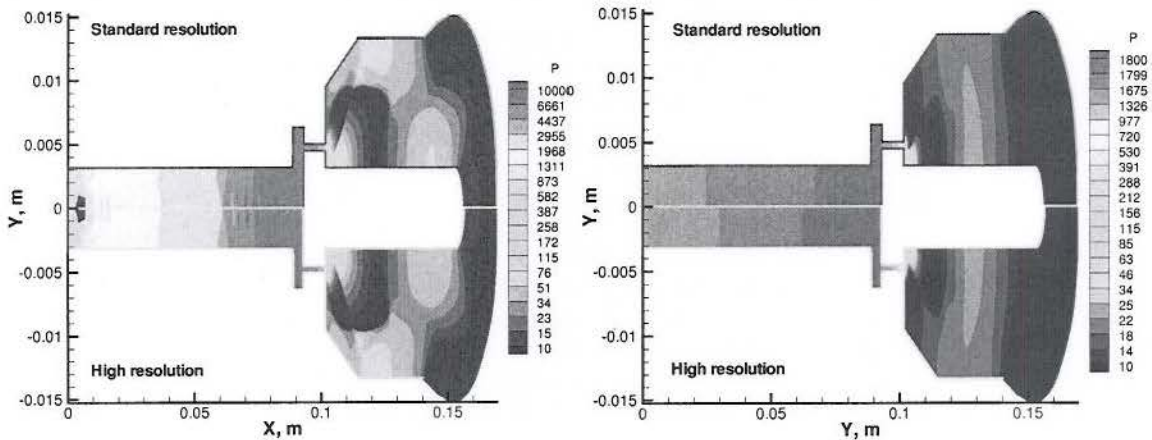

Figure 3. Comparison of pressure fields obtained with different cell size and time step at two time moments. 0.42 ms, left; 2 ms, right.

While the flow in the inlet tube is always mostly continuum, rarefaction becomes significant in the constriction and especially in the pre-ionization chamber. Slip boundary conditions of second order were therefore imposed in the Navier-Stokes computations, and a simulation with no-slip boundary conditions was also conducted for comparison. The results for the slip and no-slip cases are shown in Fig. 4 where the pressure and velocity fields are shown at 0.3 ms after the valve opening. Note some difference in the solutions. Generally, the no-slip boundary condition results in a somewhat slower motion of the compression region created in the inlet tube by the interaction of supersonic flow with the central electrode. For the slip boundary condition case, the slip velocity in the constriction was significant, up to 100 m/s near the

constriction exit. This resulted in a visibly faster flow in the pre-ionization chamber. Pressure is also somewhat higher in that region. Since the continuum approach does not allow for correct description of the gas surface interaction that a kinetic description of gas flow would allow, it contributes to the numerical uncertainty of the obtained solutions.
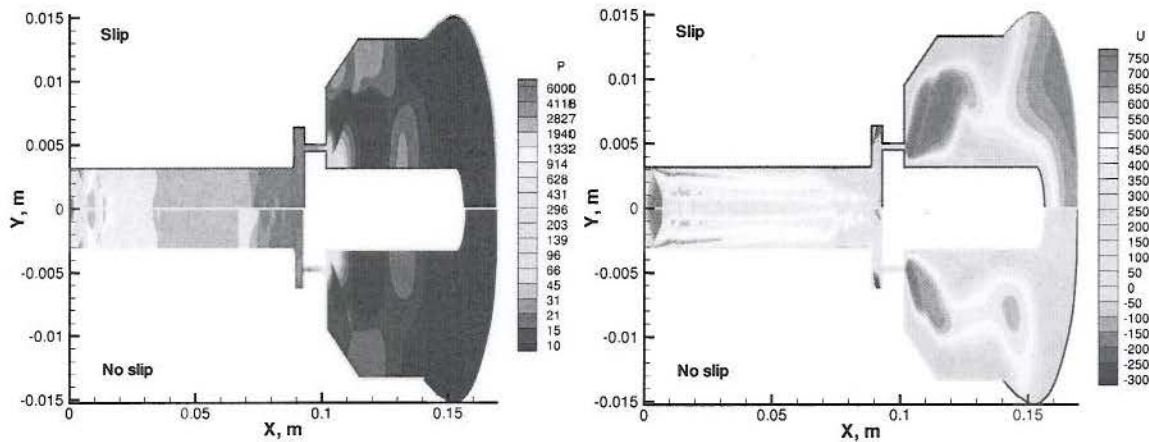

Figure 4. Impact of wall slip boundary conditions in the CFD++ solver on gas pressure (left) and axial velocity (right).

The flow in the pre-ionization chamber is rarefied enough for the DSMC method to be effectively used, and still is relatively high collision frequency, so a continuum solver can still be used. Both approaches were therefore used in that region, and a comparison between the CFD++ and Smile solutions is presented in Fig. 5 for a time moment of 0.3 ms after the valve opening. Only parts of the full Navier-Stokes and DSMC domains are given here. Note that the black region in the DSMC solution illustrates the DSMC starting surface that is located at the outer boundary of that region. The sampling (but not the collision) grid in the DSMC modeling is coarser than in the continuum simulations (a simple uniform sampling grid was used), as can be clearly seen in the figure. Note that the collisional grid in DSMC resolution is much finer than the sampling one. In this simulation, the total number of collision cells was up to 50 million, and the total number of simulated molecules up to 500 million, depending on the time moment (these numbers were found to provide grid and number of molecules independent solutions in the convergence study). The results indicate that the Navier-Stokes and DSMC solutions are very similar in the pre-ionization chamber. The difference between the two solutions is obvious only in the expansion region outside of the pre-ionization chamber, where the gas rarefaction is dominant, and the Navier-Stokes equations applicability becomes questionable. The difference is especially pronounced in the region immediately downstream from the central electrode.

IV.   Temporal evolution of flow in pre-ionization chamber

Consider now the temporal evolution of gas flow in the inlet tube and the pre-ionization chamber, shown in Fig. 6. Typical flow development in the first 2 ms after the valve opening is given in Fig. 6. At 0.1 ms, the compression front has just reached the central electrode, and started to reflect back from it. Note that there are also multiple reflections of the shock in the first half of the inlet tube. These reflections present until the valve is closed at 0.42 ms. After that time, the pressure in the inlet tube start to decrease sharply. In the pre-ionization chamber, there are several shock reflections clearly visible at 0.4 ms, although much more viscous ones than in the inlet tube (see Fig. 6a). The compression wave in that chamber first reflects on the central electrode, then on the outer wall of the pre-ionization chamber, and then again on the electrode. After the valve closing, the pressure in that chamber drops significantly, and reflections become much weaker. The gas velocity in the pre-ionization chamber is maximum at the valve closing time, reaching over 800 m/s near the outer edge of the electrode. The flow inside the inlet tube is supersonic at that time. At 2 ms, the velocity drops to less than 100 m/s in the inlet tube, and less than 500 m/s in the pre-ionization chamber.
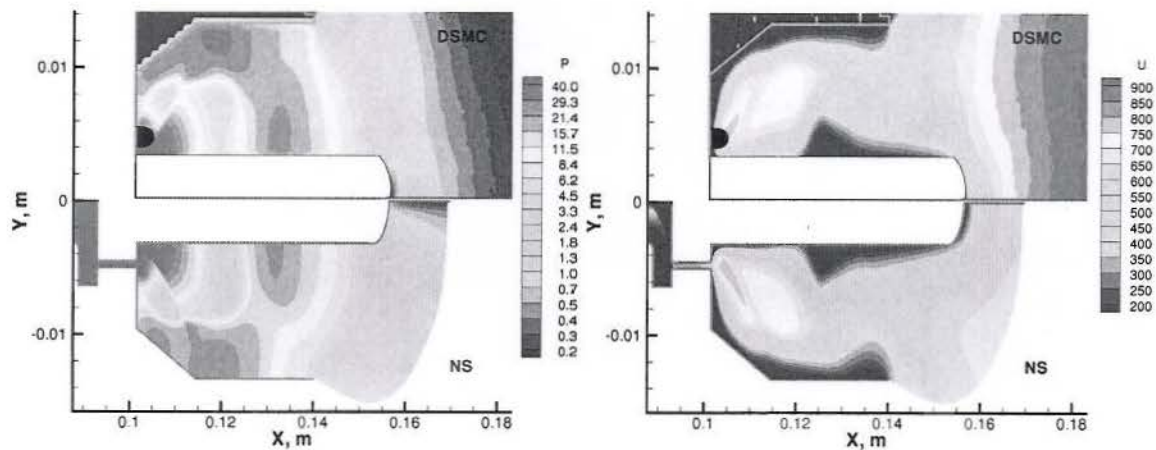
Figure 5. Gas pressure (left) and axial velocity (right) in the pre-ionization chamber obtained with different numerical approaches.
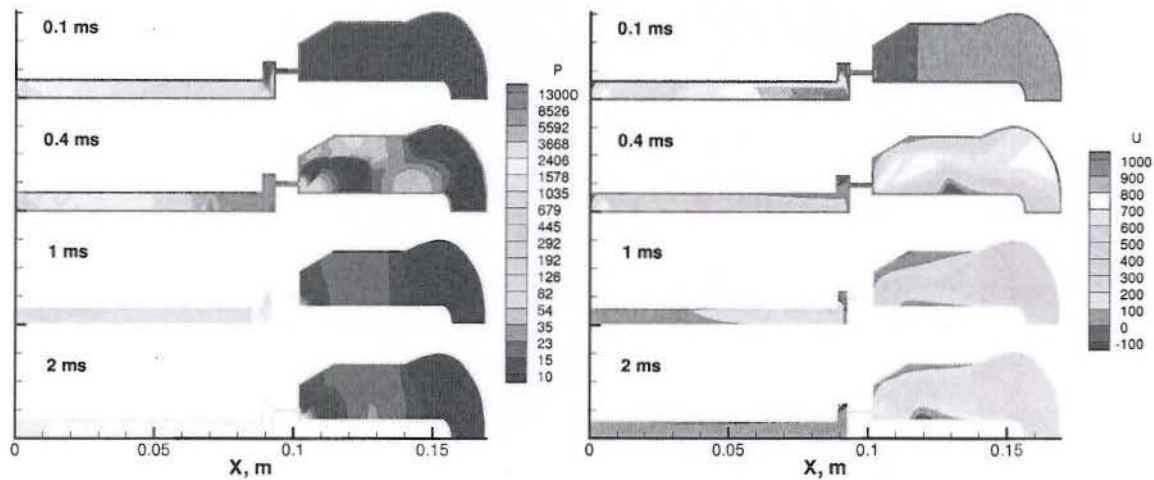

Figure 6. Temporal evolution of gas pressure (left) and velocity (right) in the pre-ionization chamber.

V.   Impact of operational parameters on flow in pre-ionization chamber

A number of chamber parameters were varied in order to analyze the sensitivity of flow properties. In this section, in addition to the baseline 0.5 mm spacing case the results are presented for a shorter valve opening time of 0.32 ms (in the experiments,[6] the valve closing took tens of microseconds, and was completed by 0.42 ms), four times lower stagnation pressure, and neon carrier gas instead of nitrogen. The results are shown in Fig. 7 where the instantaneous gas pressure and velocity are presented for four cases under consideration at 2 ms time moment. Note that here and below the pressure fields are normalized by the corresponding throat value to provide meaningful comparisons of gas relaxation for different pressures. For the shorter valve opening time, the gas pressure in the inlet tube is noticeably smaller than for the baseline case. It is interesting to note that the gas pressure in the pre-ionization chamber for that case is somewhat higher than for the baseline. This is related to the timing of reflections of compression wave from the inflow orifice and electrode walls. The compression front travels back and forth inside the inlet tube, thus decreasing and increasing pressure in the constriction opening and pre-ionization chamber. The use of neon as the carrier gas results in somewhat higher flow velocities due to its lower mass, and thus faster relaxation time as compared to molecular nitrogen. The use of lower stagnation pressure generally results in very significant delay of pressure decrease after the valve closing both in the inlet tube and in the pre-ionization chamber. This is related to dominating viscous effects inside the constriction opening, where the gas friction on the walls results in a factor of two lower velocities as compared to the baseline case. This lower flow velocity (see Fig. 7b) is responsible for a qualitatively different flow evolution for the lower pressure case.
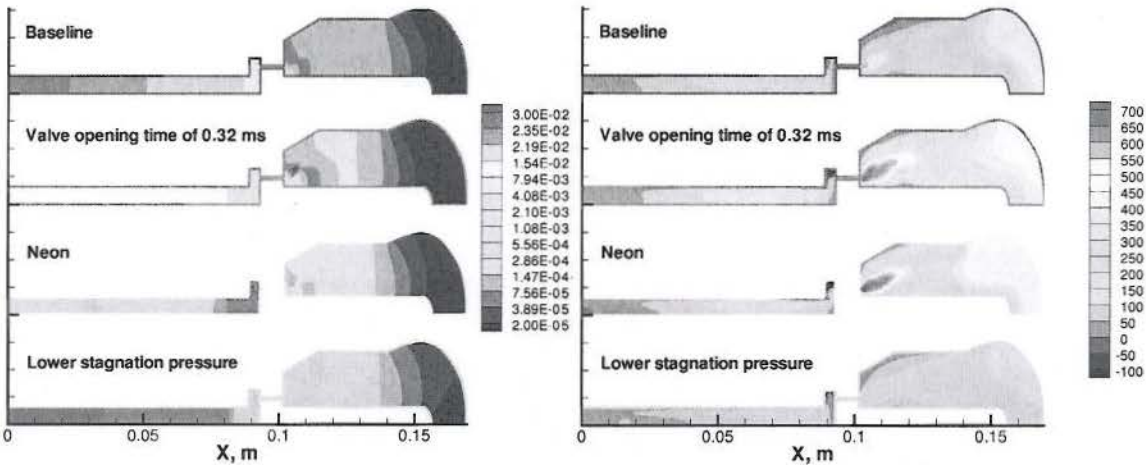

Figure 7. Impact of operational parameters on gas pressure (left) and velocity (right) in the pre-ionization chamber at 1 ms.

VI.   Temporal evolution of flow in the nozzle

The time evolution of gas expanding from the pre-ionization chamber into the diverging nozzle is shown in Fig. 8 for the 0.5 mm opening case. Both pressure and density are normalized by the corresponding throat values. After the first half a millisecond, the gas flow from orifice has reached the middle part of the nozzle. Note that in that part, the pressure in the radial direction is maximum near the nozzle wall. This pressure maximum is caused by the compression wave that reflects on the central electrode and propagates outward to the nozzle surface. After the reflection on the nozzle wall, it travels inward to the nozzle axis, as clearly seen at 1 ms time moment. After that, the rest of the nozzle is filled, and at about 3 ms after the valve opening the pressure gradient in the nozzle is relatively small, especially in the radial direction. Note that the both in pre-ionization chamber and inside the nozzle starts to decrease after about 2 ms due to decreasing pressure in the inlet tube.

For the ionization stage of thruster operation, it is important to know the the pressure and especially the number density in the second half of the nozzle and near the nozzle exit plane, where the ionization is

expected to take place. For the FRC formation to be efficient, it is desirable to have relatively uniform radial pressure distribution in that region. Whereas the pressure is indeed relatively uniform (see Fig. 8a), with the difference between axis and wall values not exceeding about 30%, the density is up to a factor of two higher near the axis than near the wall for any given axial location, as illustrated in Fig. 8b.
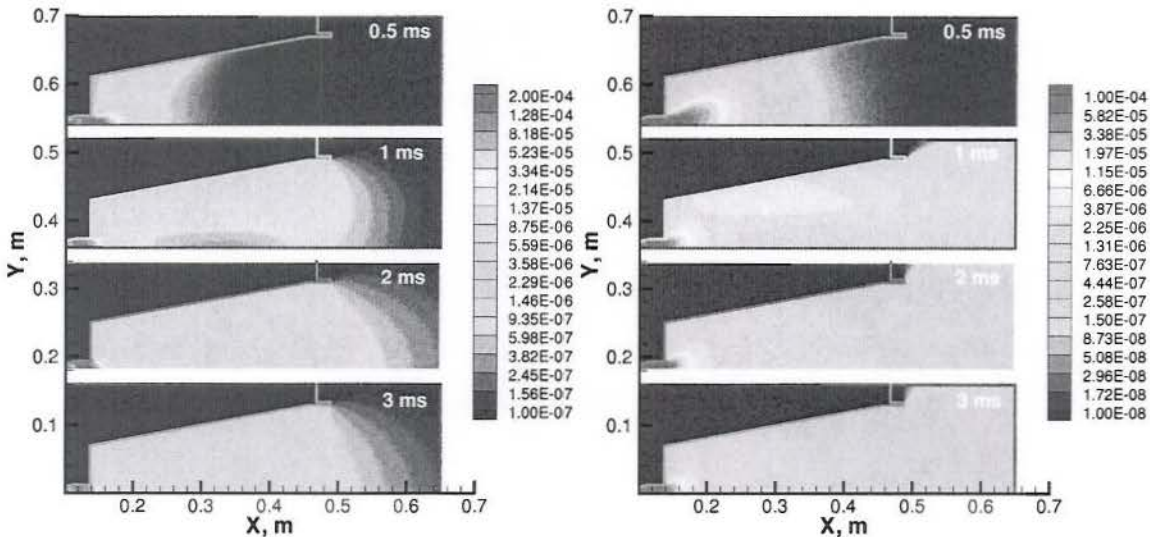

Figure 8. Temporal evolution of gas pressure (left) and number density (right) in the nozzle.

VII. Impact of operational parameters on flow in the nozzle

The results of the modeling have shown that pressure in the nozzle ranges from single digit values near the pre-ionization chamber to a fraction of a Pascal near the nozzle exit. That means that the Knudsen number based on the radial dimension of the nozzle is on the order of 0.1. Such a high Knudsen number is characterized by the strong impact of the nozzle surface. While the gas-surface interaction was assumed to be fully diffuse and surface temperature assumed to be 300 K, and additional calculation was conducted with specularly reflective wall to illustrate the impact of the nozzle surface. While the diffuse reflection clearly much better approximates real gas-surface interactions, such a comparison nevertheless provides an upper limit for the wall model related numerical uncertainty. The results of the comparison are summarized in Fig. 9.

The wall specularity significantly reduces the gas pressure inside the nozzle. This is related to the fact molecules reflected on a specular wall keep the tangential components of their velocity, and thus mostly move toward the nozzle exit after being reflected. This in turn reduces gas temperature and increases axial velocity, therefore reducing temperature and pressure, as seen in Fig. 9a. Higher velocity also strongly reduces gas density, with the maximum difference at the axis approaching a factor of four. All this illustrates the importance of accurate modeling of gas-surface interactions at the nozzle wall.

The impact of different chamber parameters is illustrated in Fig. 10. Shorter valve opening time impacts only the slightly the gas properties at 2 ms, and the results are qualitatively similar to the baseline case. The use of neon as carrier gas also does not result in any significant change of gas properties in the nozzle. The decrease in stagnation pressure result in the increase of the exit radius based Knudsen number to about 1; in this case, the flow properties (both pressure and density) are fairly uniform in the radial direction. Increase in the radial dimension of the nozzle causes nearly proportional reduction in gas pressure and density near the nozzle exit.

The flow properties along the nozzle exit plane are shown in Fig. 11 for different chamber conditions. Here, X=0 corresponds to the nozzle axis. These results show that the gas pressure, Fig. 11a, is nearly constant for the lower pressure, and is still relatively flat for the shorter valve opening time and neon carrier gas. As expected, the pressure is least uniform for the baseline case, for which the absolute values of pressure
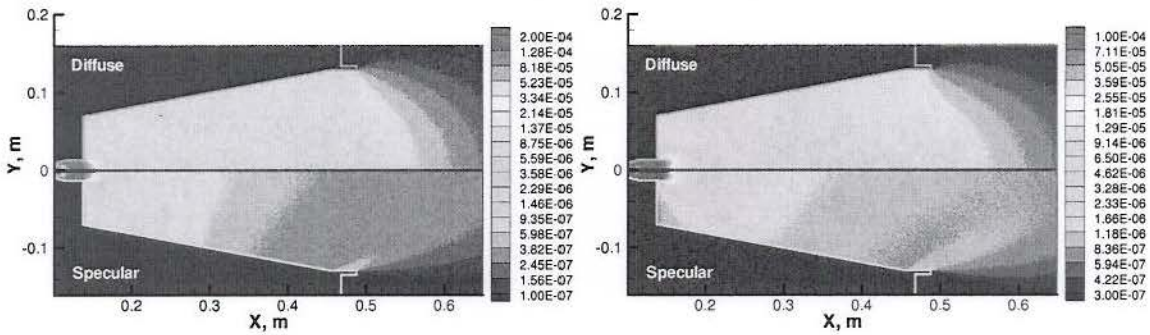
Figure 9. Impact of gas-surface interaction model on gas pressure (left) and number density (right) in the nozzle at 2 ms.
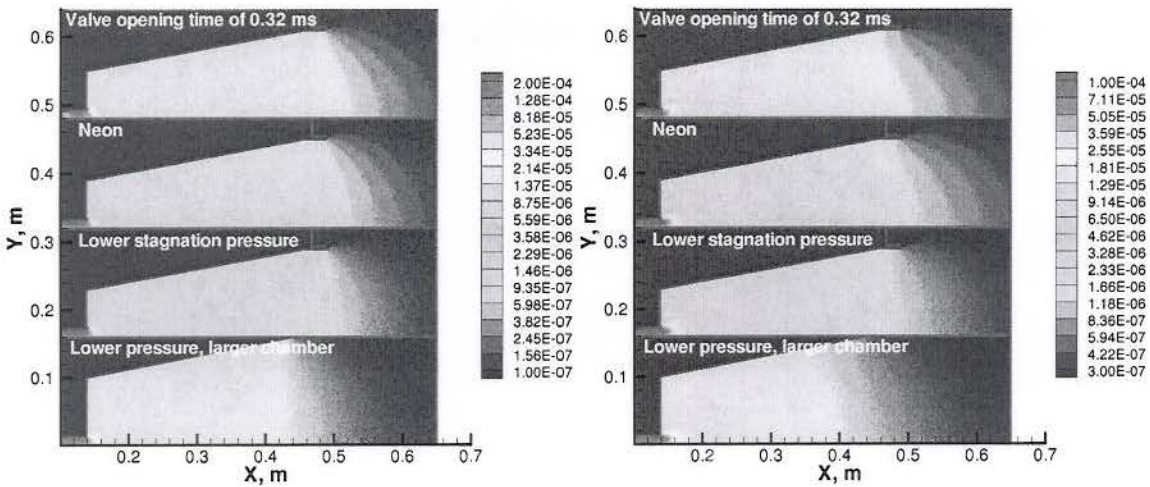

Figure 10. Impact of operational parameters on gas pressure (left) and number density (right) in the nozzle at 2ms.

are also maximum. This trend is also true for the number density (Fig. 11b). Note also that the diffuse reflection model along with fairly high rarefaction were found to nearly nearly constant gas temperatures of about 300 K at the nozzle exit plane.
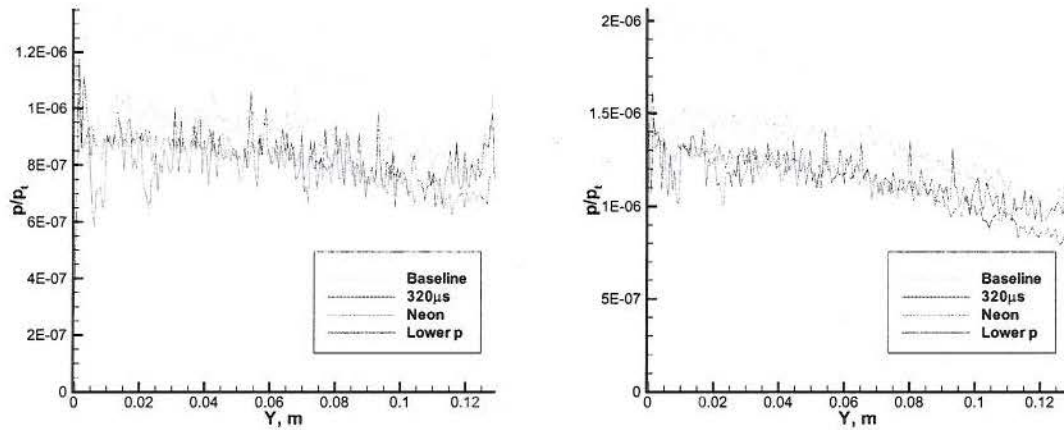

Figure 11. Gas pressure (left) and number density (right) along the nozzle exit plane at 2ms.

VIII. Steady state flow

The process of gas ionization and FRC plasmoid formation with its successive translation out of the nozzle is conducted in a pulsed regime, with the ionization stage typically taking a few microseconds and plasmoid formation and translation, a few tens of microseconds. The neutral injection, however, may operate both in a pulsed and quasi-steady state regime. In order to provide an estimate on gas properties in the FRC nozzle for the latter, a steady state computation has been conducted using the same continuum/kinetic approach employed for the above transient simulations, with one exception that the starting surface for the DSMC modeling was obtained from a converged steady-state Navier-Stokes computation. Note that the convergence process was slow, and it took almost 20 million timesteps to complete. The results of the steady state simulation are presented in Fig. 12, where normalized pressure and density fields are shown. The most important conclusion here is that, since the steady state operation results in noticeably higher gas density and thus collision rates in the nozzle, there is a compression front clearly visible that reflects on the nozzle wall and falls back on the axis near the nozzle exit. This results in significant non-uniformity of gas properties at the nozzle exit plane, with the maximum difference noticed in the number density of about a factor of three.
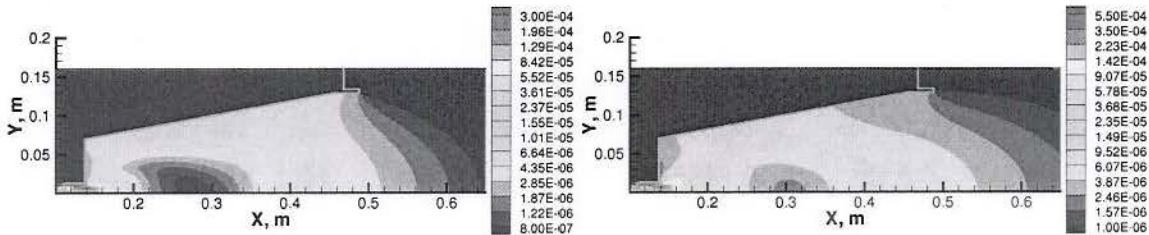

Figure 12. Gas pressure (left) and number density (right) for the steady state case.

IX. Acknowledgments

References

[1] McKenna K.F. et al., "Particle confinement scaling in field-reversed configurations", Phys. Rev. Lett. 50, 1787 (1983)

[2] Rostoker N. and Qerushi A., "Classical transport in a field reversed configuration", Plasma Phys. Rep. 29(7), 626 (2003).

[3] Elliott F., Foster J., and Patterson M., An Overview of the High Power Electric Propulsion (HiPEP) Project, AIAA Paper 2004-3453.

[4] Kirtley D., Brown D., and Gallimore A. Details on an annular field reversed configuration plasma device for spacecraft propulsion, IEPC-2005-171.

[5] Miller S., Rovey J. Progress in modeling of pre-ionization and geometric effects on a field-reversed configuration plasma thruster, AIAA 2009-3733.

[6] Slough J., Kirtley D., and Weber T. Pulsed plasmoid propulsion: the ELF thruster, IEPC-2009-265.

[7] J. Slough and D. Kirtley, Nuclear Propulsion based on Inductively Driven Liner Compression of Fusion Plasmoids, AIAA Aerospace Sciences (2011).

[8] Chakravarthy S. and Peroomian O. Some internal flow applications of a unified-grid CFD methodology, AIAA Paper 96-2926.

[9] Ivanov M.S., Markelov G.N., and Gimelshein S.F. Statistical simulation of reactive rarefied flows: numerical approach and applications, AIAA Paper 98-2669.